J. Biochem. 131, 267–275 (2002)

Real-Time Kinetic Analyses of the Interaction of Ricin Toxin A-Chain with Ribosomes Prove a Conformational Change Involved in Complex Formation[1]

Eijiro Honjo, Keiichi Watanabe,[2] and Takuji Tsukamoto

Department of Applied Biological Sciences, Saga University, Saga 840-8502

Received October 15, 2001; accepted December 6, 2001

Ricin toxin A-chain (RTA), a ribosome-inactivating protein from seeds of the castor bean plant (*Ricinus communis*), inactivates eukaryotic ribosomes by hydrolyzing the *N*-glycosidic bond of a single adenosine residue in a highly conserved loop of 28S rRNA, but does not act on prokaryotic ribosomes. We investigated the interaction of rat liver 80S ribosomes with RTA using an optical biosensor based on surface plasmon resonance (BIAcore instrument), which allows real-time recording of the interaction. RTA was coupled to the dextran gel matrix on the sensor chip surface through a single thiol group that is not involved in the enzymatic action. The interaction of rat ribosomes with RTA, which was greatly affected by the Mg^{2+} concentration and ionic strength, was usually measured at 5 mM Mg^{2+}, 50 mM KCl, and pH 7.5. The modes of interaction of intact and RTA-depurinated rat liver ribosomes with the immobilized RTA were virtually the same, while no considerable interaction was observed for *Escherichia coli* ribosomes. The interaction was not influenced by the presence of 5 mM adenine, which is higher than the reported dissociation constant (1 mM) for the adenine-RTA complex. These results demonstrate that binding of the target adenine with the active site of RTA does not contribute much to the total interaction of ribosomes and RTA. Global analyses of association and dissociation data with several binding models, taking account of mass transport, allowed us to conclude that the data were unable to fit a simple 1:1 binding model, but were best described by a model including a conformational change involved in high affinity complex formation.

Key words: BIAcore, ribosome-inactivating protein, ricin A-chain, RNA *N*-glycosidase, surface plasmon resonance.

Ricin toxin is a heterodimeric protein from seeds of the castor bean plant (*Ricinus communis*) consisting of an A-chain (RTA, 267 residues) and a B-chain (RTB, 262 residues) linked by a single disulfide bond (reviewed in Ref. *1*). RTB binds to galactose-containing receptors on the cell surface and RTA inactivates ribosomes by hydrolyzing the *N*-glycosidic bond of a single adenosine residue in a highly conserved domain [sarcin/ricin (S/R) domain] of 28S rRNA (A4324 in rat 28S rRNA) (*2*). The conserved purine-rich sequence of 12 nucleotides in the S/R domain forms a GAGA tetraloop containing the target adenine (the first A) and a G-bulged cross-strand A stack (*3–5*), and is known to be essential for the binding of elongation factors (*6*). Although RTA exhibits strong activity on mammal ribosomes, it is not able to act on *E. coli* ribosomes in spite of the existence of the target S/R domain (*7, 8*). Ribosome-inactivating proteins (RIPs) having the same enzymatic activity as RTA have been found in a wide variety of plants and two species of bacteria (*7, 8*). In contrast to RTA, many other RIPs exist as a monomer and depurinate not only eukaryotic but also prokaryotic ribosomes. X-ray crystallographic studies, comparison of the amino acid sequence of RTA with those of other RIPs, and mutational analyses have proved that a prominent cleft in RTA is an active site (*1*). The concerted actions of Glu177, Arg180, and an activated water molecule at the cleft have been proposed to catalyze the depurination (*1, 9*). With the ultracentrifugation technique, it has been shown that RTA binds rat liver ribosomes with a molar stoichiometry of 1:1 and a dissociation constant of 6.2×10^{-8} M at 5.5 mM Mg^{2+} (*10*). However, analyses of RTA-ribosome interactions have so far been limited to those in an equilibrium state and there has been no report on the analysis of association and dissociation kinetics. Such kinetic analysis would provide us with important information for understanding the enzymatic action of RTA in detail, that is, from an initial step of RTA-ribosome association to a final step of dissociation of RTA from the product (depurinated) ribosome.

Optical biosensors based on surface plasmon resonance

[1]This work was supported by a Grant-in-Aid for Scientific Research from the Ministry of Education, Science, Sports and Culture of Japan.

[2]To whom correspondence should be addressed. Tel/Fax: +81-952-28-8774, E-mail: watakei@cc.saga-u.ac.jp

Abbreviations: RTA, ricin toxin A-chain; RTB, ricin toxin B-chain; RIP, ribosome-inactivating protein; SPR, surface plasmon resonance; NHS, *N*-hydroxysuccinimide; EDC, *N*-ethyl-*N'*-(3-dimethylaminopropyl)carbodiimide; MBS, *N*-(4-maleimidobutyryloxy)succinimide; DTT, dithiothreitol; MTL, mass transport limitation; PAP, pokeweed antiviral protein.

(SPR) have become popular for determining the affinity and kinetics of the interactions of biological macromolecules (reviewed in Refs. *11–13*). In BIAcore instruments (*14*), the sensor surface is composed of an optically flat glass with a gold film deposited on one side, which is covered with a covalently bound dextran gel matrix. The ligand is coupled to the dextran matrix, this side coming into contact with the bulk solution, and the glass side is illuminated with a near infra-red light. As the analyte from the bulk flow binds to the immobilized ligand, the index of refraction at the surface changes, which affects the incident light angle at which SPR is observed. Thus SPR appears as a dip in the intensity of the light reflected from the surface at a specific incident angle, which is converted to a response proportional to the mass bound to the surface and expressed in resonance units (RU). The continuous monitoring of the SPR response allows the association process to be followed in real time. The dissociation kinetics may be monitored by the introduction of buffer alone after binding.

In this study, to investigate the real-time kinetics of the RTA-ribosome interaction, we immobilized RTA on the sensor surface through a single solvent-exposed thiol group and then analyzed the SPR signals derived from ribosomes bound to the surface. Our careful examination of the interactions allowed us to conclude that a conformational change is involved in the formation of the RTA-ribosome complex.

MATERIALS AND METHODS

Materials—A BIAcore biosensor system and sensor chip CM5 were purchased from Pharmacia Biosensor AB. *N*-Hydroxysuccinimide (NHS), *N*-ethyl-*N'*-(3-dimethylaminopropyl)carbodiimide (EDC), and *N*-(4-maleimidobutyryloxy)succinimide (MBS) were from Wako Pure Chemicals (Tokyo). *E. coli* XL-1 blue was from Stratagene, the pKK223-3 plasmid was from Amersham Pharmacia Biotech, and SP-Toyopearl 550C was from Tosoh.

Preparation of Recombinant RTA—The RTA gene was obtained from the genomic DNA of *Ricinus communis* by means of a polymerase chain reaction involving two specific primers based on the known genomic sequence of RTA (*15*). *E. coli* XL-1 blue was transformed with the pKK223-3 plasmid including the RTA gene. The expression of recombinant RTA was induced in the transformant at 25°C for 24 h after the addition of 1 mM isopropyl-β-D-thiogalactopyranoside to the culture. The extract obtained with the combination of lysozyme-treatment and sonication of *E. coli* cells was applied on a SP-Toyopearl 550C column equilibrated with 10 mM Na phosphate, pH 6.5, 1 mM EDTA, 10 mM 2-mercaptoethanol, and 5% glycerol. The RTA, eluted from the column with a linear gradient of NaCl, from 0 to 0.4 M, was dialyzed against 50 mM $(NH_4)_2SO_4$ and 10 mM 2-mercaptoethanol in Milli-Q water (pH 6.5), concentrated to 6 mg/ml, and then stored at –80°C. The RTA concentration was measured by a method of Lowry *et al.* (*16*) using bovine serum albumin as a standard.

Preparation of Rat Liver 80S and E. coli 70S Ribosomes—Rat liver 80S ribosomes were prepared by the established procedure involving puromycin treatment of crude polysomes (*17*). Depurinated ribosomes were obtained by incubation of 80S ribosomes (100 A_{260} units/ml) with RTA (0.33 nM) in 5 mM Tris-HCl, pH 7.5, 50 mM KCl, 5 mM Mg acetate, and 1 mM dithiothreitol (DTT) at 37°C for 30 min, followed by ultracentrifugation through a sucrose cushion containing 0.3 M KCl. The concentration of rat liver ribosomes was determined by assuming 17 pmol/A_{260} unit.

E. coli 70S ribosomes were obtained by ultracentrifugation of the S30 supernatant. The S30 supernatant was centrifuged at 230,000 ×*g* for 4 h through discontinuous sucrose gradients consisting of 0.4 and 1.2 M sucrose in 20 mM Tris-HCl, pH 8.0, 10 mM Mg acetate, 20 mM NH_4Cl, and 5 mM 2-mercaptoethanol. The resulting pellet was resuspended in 20 mM Tris-HCl, pH 7.6, 10 mM Mg acetate, 1 M NH_4Cl and 5 mM 2-mercaptoethanol, followed by centrifugation at 230,000 ×*g* for 3 h. The resuspension and centrifugation procedure was repeated an additional 3 times. The pellet was resuspended in 5 mM Tris-HCl, pH 7.5, 50 mM KCl, 5 mM Mg acetate, and 1 mM DTT, and then stored at –80°C. The concentration of *E. coli* ribosomes was determined by assuming 26 pmol/A_{260} unit.

Immobilization of RTA—Immobilization of RTA on the surface of the sensor chip CM5 was obtained either through amino groups or through a single thiol group of RTA using a BIAcore instrument at 25°C. The carboxymethylated dextran matrix, equilibrated with 10 mM Hepes, pH 7.4, 150 mM NaCl, and 3.4 mM EDTA (HBS), was activated by injection of 35 μl of a 0.05 M NHS/0.2 M EDC mixture (*18*) in Milli-Q water for 7 min at the flow rate of 5 μl/min. After replacement of the buffer on the flow cell with 10 mM Na acetate, pH 6.0, and 0.15 M NaCl (ABS) using the INITIATE command, RTA (400 μg/ml in ABS) was injected for 10 min at 5 μl/min so as to be immobilized through its amino groups. Unreacted NHS-esters on the sensor surface were blocked by injection of 1.0 M ethanolamine (pH 8.5) for 7 min at 5 μl/min.

Alternatively, RTA was immobilized through a thiol group on the sensor surface modified by introduction of reactive maleimide groups (*19*). After activation of the surface with NHS/EDC as described above, amino groups were generated by injection of 1.0 M ethylene diamine (pH 6.0) for 10 min at 5 μl/min. To introduce maleimide groups, the sensor surface was exposed to 15 mM MBS in HBS/ethanol (1:1) for 30 min at 5 μl/min. After replacement of the buffer on the flow cell with ABS, RTA (800 μg/ml in ABS) was injected for 25 min at 2 μl/min. Unreacted maleimide groups were blocked by injection of 10 mM DTT for 2 min at 5 μl/min. At the end of each immobilization run, 40 μl of 20 mM Tris-HCl, pH 7.5, 1 M KCl, 1 mM EDTA, and 1 mM DTT was injected at 5 μl/min to wash the sensor surface. A level of about 5,000 RU of RTA, corresponding to a surface concentration of 5 ng/mm^2 (*20*), was usually immobilized with both the methods. The injection time for the RTA solution was changed to alter the immobilization level when required. Control surfaces were prepared by the same procedures as for RTA immobilization but without the injection of RTA.

Recording of Sensorgrams—The interactions of ribosomes with immobilized RTA were measured at 25°C by monitoring real time changes in SPR using a BIAcore instrument. Ribosomes (1–400 nM) in the standard running buffer (5 mM Tris-HCl, pH 7.5, 50 mM KCl, 5 mM Mg acetate, and 1 mM DTT) were injected over a RTA-immobilized surface for 240 s at 5 μl/min. The dissociation of bound ribosomes was allowed to proceed for 220 s with a 5

μl/min flow of the standard running buffer containing no ribosomes. The sensor surface was regenerated after each association and dissociation cycle by injecting 20 mM Tris-HCl, pH 7.5, 1 M KCl, 1 mM EDTA, and 1 mM DTT for 8 min at 5 μl/min, and then initialized with a continuous flow of the running buffer for 2 min prior to the start of the next run cycle. Neither accumulation of the bound ribosomes nor reduction of the response was observed on up to 20 repeated runs. Background sensorgrams were obtained by injection of the same concentration of ribosomes over the control surface for subtraction of the bulk refractive index values and nonspecific binding.

Measurement of Mass Transport Limitation (MTL)—The contribution to the observed binding rate of ribosomal mass transport from the bulk flow to the RTA surface was determined from the effect of a change in the flow rate on the apparent initial binding rate using a BIA-CONC program (*21*). The theory for and application of this method were reported by Christensen (*22*) and Richalet-Sécordel *et al.* (*21*), respectively. For this method, the binding is treated as two successive processes: transport of the analyte in the bulk (A_{bulk}) to the sensor surface ($A_{surface}$), followed by binding of $A_{surface}$ to immobilized ligand B, which is referred to as a two-compartment model. Assuming that a quasi-steady state with $d[A_{surface}]/dt = 0$ exists and that at the beginning of the association phase the effect of dissociation on the binding can be neglected, the binding rate (response slope) can be expressed by the equation:

$$dR/dt = L_m \cdot L_r \cdot MW \cdot G \cdot [A_{bulk}]/(L_m + L_r), \quad (1)$$

where $[A_{bulk}]$ is the analyte concentration (mol/m^3 = 10^6 nM), R is the response level (RU), MW is the molecular weight of the analyte (g/mol), G is the response per mass per area (RU·m^2/g = 10^{-3} RU·mm^2/ng), L_m is the mass transport coefficient (m/s), and L_r is the Onsager coefficient of reaction flux (m/s) (*23*). L_m with detection between distances l_1 and l_2 from the inlet of the flow cell is given by the expression (*21*):

$$L_m = 1.47 \cdot \frac{1-(l_1/l_2)^{2/3}}{1-l_1/l_2} \cdot \sqrt[3]{\frac{D^2 \cdot F}{h^2 \cdot b \cdot l_2}} \quad (2)$$

where D is the diffusion coefficient of the analyte (m^2/s), h and b are the height and width of the flow cell (m), and F is the bulk flow rate (m^3/s = 6×10^{10} μl/min). Thus, L_m is proportional to the cubic root of the flow rate. G for protein is approximately 1,000 RU·mm^2/ng (*20*), but that for ribosomes is not known. When MW and the analyte concentration $[A_{bulk}]$ are known, G and L_r can be determed with Eq. 1 with the response slopes, dR/dt, obtained by linear regression with various values of L_m. A quantitative measure of the mass transport limitation (MTL) can be expressed as:

$$MTL = L_m/(L_m + L_r). \quad (3)$$

When no mass transport limitation exists, the MTL value is zero, and when mass transport totally dominates binding, it is one.

The concentration of rat liver ribosomes (4 nM) was selected to give an initial binding rate in the range of 1 to 10 RU/s with flow rates of 5–50 μl/min. The ribosomes (40 μl) were injected over the sensor surface with 4,780 RU of immobilized RTA at 5, 10, 25, and 50 μl/min, followed by the regeneration step. The sensorgrams of the postinjection and regeneration phases were deleted, and then the base line of sensorgrams was adjusted to 0 RU using a BIAevaluation 3.0 program (BIACORE). The arranged sensorgrams were exported to the BIA-CONC program to analyze the mass transport effect on the binding, as well as to evaluate G for ribosomes. The values inputted for the calculation of results were: MW of rat liver ribosomes, 4.3×10^6 g/mol (*24*); D for eucaryotic ribosomes, 1.41×10^{-11} m^2/s (*25*); and cell dimensions $h = 5 \times 10^{-5}$ m, $b = 5 \times 10^{-4}$ m, $l_1 = 4 \times 10^{-4}$ m, and $l_2 = 2 \times 10^{-3}$ m. The times of the beginning of specific interactions after bulk refractive index changes were determined from the sensorgrams obtained by injecting ribosomes over the control surface. The number and height of RU intervals, for which slopes, dR/dt, were measured by linear regression, were selected as suggested in Ref. *21*.

Kinetic Data Analysis—The obtained sensorgrams including association and dissociation phases were analyzed by globally fitting the binding model to the data using BIAevaluation 3.0. Before the fitting procedure, the base lines and the start times of association phases were adjusted to 0 RU and 0 s, respectively, for all sensorgrams, and then the background data were subtracted from the corresponding sample data. Attempts were made to globally fit not only the 1:1 binding model but also more complicated ones, predefined in the software, to the obtained data together with the two-compartment model for the treatment of mass transport (*26*). The mass transport rate constant k_t (s^{-1}), used in the predefined model, is related to the mass transfer coefficient, L_m (m/s) by the expression:

$$k_t = 10^6 \cdot G \cdot MW \cdot L_m, \quad (4)$$

where the unit of G is RU·mm^2/ng. The bivalent analyte model describes the binding of a bivalent analyte (ribosome) to an immobilized ligand (RTA), where one ribosome can bind to one or two RTA molecules. In the heterogeneous analyte (competing reactions) model, two different populations of ribosomes compete for the same immobilized RTA. The heterogeneous ligand (parallel reactions) model describes independent and parallel interactions between ribosomes and two different populations of immobilized RTA. The two-state (conformational change) model describes 1:1 binding of ribosomes to immobilized RTA, followed by a reversible conformational change in the complex.

RESULTS

Immobilization Methods—The RTA molecule contains three accessible amino groups (Lys4, Lys239 and N-terminus) and one solvent-exposed thiol group of Cys259 that participates in a disulfide bond to RTB. Chemical modification of either the amino groups or the thiol one of RTA has been reported to have no influence on the ribosome-inactivating activity (*10*). RTA was, therefore, immobilized on the dextran matrix of sensor surfaces through the amino groups or the thiol one to examine the influence of these immobilization methods on the interaction with ribosomes. Levels of 5,300 and 6,380 RU of RTA were immobilized on separate surfaces by the thiol- and amine-coupling methods, respectively. Figure 1 shows the sensorgrams obtained by injection of 25 nM rat liver 80S ribosomes over each surface. The refractive index contributions from the bulk solvent and nonspecific binding of ribosomes to the dextran

matrix were determined from the sensorgram obtained by injection of the same concentration of ribosomes over each control surface. Both background responses were approximately 200 RU (Fig. 1). In spite of the lower level of the thiol-immobilized RTA, the response on this surface at an injection time of 4 min (3,080 RU) was 1.6-fold higher than that on the amine-immobilized RTA. This result indicates that the RTA-immobilization through a single thiol group is more suitable for the interaction with ribosomes than the nonspecific immobilization through amino groups. Therefore, the thiol-immobilization method was employed in the following experiments.

It should be noted that no response derived from the ribosome-RTA interaction was observed when the level of immobilized RTA was lower than about 1,000 RU. This can be explained by the assumption that ribosomes can only gain access to the ligand present on the gel surface, *i.e.* not to that within the gel, because of its very large size, although the dextran matrix (thickness of approximately 100 nm) has been shown not to act as a molecular sieve for an antibody having a molecular mass of 150 kDa (*20*). At an immobilization level of 1,000 RU (corresponding to a surface concentration of 1 ng/mm^2), a negligible amount of RTA molecules may appear on the gel surface, while at an immobilization level of 5,000 RU, there are some RTA molecules present on the gel surface, which can interact with ribosomes.

Effects of Ionic Concentrations on the Interaction—The effects of the concentrations of Mg^{2+} and KCl on the interaction of rat liver 80S ribosomes with the immobilized RTA were investigated. As shown in Fig. 2A, the Mg^{2+} concentration (2–18 mM) in the presence of 50 mM KCl had a large effect on the association phase. Increasing the Mg^{2+} concentration from 2 to 16 mM caused concomitant enhancement of the response at an injection time of 4 min, the response at 16 mM Mg^{2+} being 10-fold higher than that at 2 mM Mg^{2+}, while the association rate appeared to be reduced at Mg^{2+} concentrations above 10 mM. As seen from the dissociation phases, the dissociation rate appeared to continuously decrease with an increase in Mg^{2+} concentration from 2 to 16 mM. At a much lower concentration of KCl (5 mM), increasing the Mg^{2+} concentration from 2 to 18 mM resulted in a continuous increase in the overall response and a continuous decrease in the dissociation rate (Fig. 2B).

The influence of KCl in the range of 20 to 100 mM on the interaction was examined at 5 and 15 mM Mg^{2+}. The observed effect of KCl was affected by the Mg^{2+} concentration (Fig. 3, A and B). At 5 mM Mg^{2+}, varying the KCl concentration from 40 to 80 mM had little effect on the interaction, while at 20 mM or 100 mM KCl, a distinct increase in the response was observed (Fig. 3A). Such an obvious change in the interaction at 100 mM KCl disappeared in the presence of 15 mM Mg^{2+} (Fig. 3B). Furthermore, the KCl concentration giving the lowest response shifted from 40 to 60 mM with an increase in Mg^{2+} concentration from 5 to 15 mM. Thus changes in the Mg^{2+} and KCl concentrations mutually affected their influences on the interaction of RTA with ribosomes. We used 5 mM Tris-HCl buffer (pH 7.5) containing 50 mM KCl, 5 mM Mg acetate, and 1 mM DTT as a standard running buffer because it was the same as that we used for enzymatic assaying of RTA and similar to that used for cell-free protein synthesis.

The ionic strength of the running buffer may influence the sensorgram not only by affecting the intrinsic ionic interactions between immobilized ligand and analyte mole-

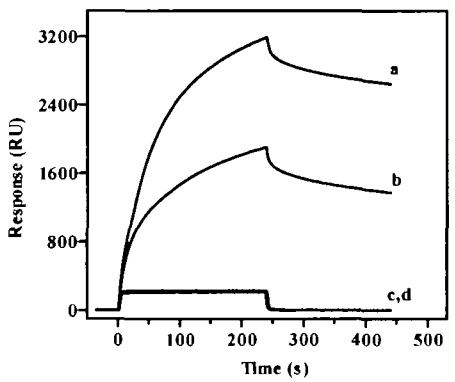

Fig. 1. **Effect of the coupling method on the binding of rat liver 80S ribosomes to immobilized RTA.** Solutions of 25 nM ribosomes in the standard running buffer (5 mM Tris-HCl, pH 7.5, 50 mM KCl, 5 mM Mg acetate, and 1 mM DTT) were injected for 4 min at the flow rate of 5 μl/min at 25°C over two separate surfaces on which 5,300 and 6,380 RU of RTA had been immobilized by the thiol-coupling (a) and amine-coupling (b) methods, respectively. The dissociation of bound ribosomes was performed for 220 s with a 5 μl/min flow of the standard running buffer containing no ribosomes. C and d indicate the control sensorgrams for a and b, respectively, which were obtained by injection of ribosomes over control surfaces.

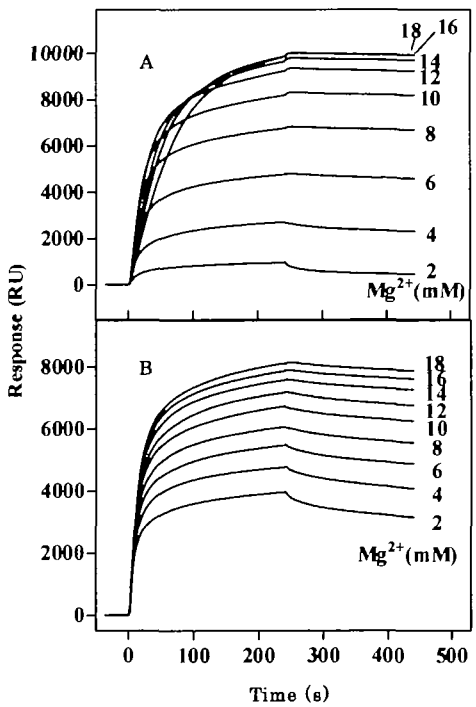

Fig. 2. **Effect of the Mg^{2+} concentration on the binding of rat liver 80S ribosomes to immobilized RTA in the presence of 50 mM (A) or 5 mM (B) KCl.** The Mg^{2+} concentration in the running buffer was varied from 2 to 18 mM, as indicated in the figure. The ribosomes (100 nM) in each running buffer were injected over the RTA surface (5,700 RU immobilized) for 4 min at 5 μl/min. The dissociation of bound ribosomes was performed for 220 s with a 5 μl/min flow of the same running buffer containing no ribosomes. The responses obtained on the control surface were subtracted from those on the RTA-immobilized surfaces.

cules but also by altering the non-specific binding of unactivated negatively charged carboxyl groups of the dextran matrix with either positively charged analytes or ligands. In the present system, such nonspecific electrostatic binding to the dextran is likely to be negligible, because ribosomes and RTA [p*I* = 7.6 (*7*)] have a negative and almost no net charge, respectively, in the standard running buffer. It is well known that Mg^{2+} and ionic strength affect the structure and function of ribosomes. The observed effects of the Mg^{2+} and KCl concentrations on the ribosome-RTA interaction may be due to their influences on the ribosomal structure. It should be emphasized, therefore, that the characteristics of the interaction with ribosomes should be stated together with the experimental ionic conditions.

Interaction of Depurinated Rat Liver 80S Ribosomes and E. coli 70S Ribosomes with Immobilized RTA—RTA depurinates eukaryotic ribosomes at a specific adenosine residue on 28S rRNA (A4324 in rat liver ribosomes). As shown in Fig. 4, the mode of interaction of depurinated rat liver ribosomes (product ribosomes obtained after complete reaction with RTA) was essentially the same as that of intact ribosomes. Furthermore, neither association of ribosomes with RTA nor dissociation of their complex was affected by the presence of 5 mM adenine, which is higher than the reported dissociation constant (1 mM) for the adenine-RTA complex (*27*). These results demonstrate that the interaction of the target adenine with the active site of RTA does not contribute much to the total interaction of ribosomes with RTA. Other parts of rRNA as well as ribosomal proteins may participate in the interaction. On the other hand, no significant interaction was observed for *E. coli* ribosomes (Fig. 4). This failure of RTA to bind to *E. coli* ribosomes is consistent with the fact that RTA can not act on *E. coli* ribosomes as an *N*-glycosidase in spite of the existence of the target adenine, at which some other RIPs such as pokeweed antiviral protein (PAP) are able to hydrolyze the *N*-glycosidic bond (*7, 8*).

Kinetics of the Interaction of Rat Liver 80S Ribosomes with Immobilized RTA—If the binding of an analyte to an immobilized ligand is fast, the observed binding might be influenced by the analyte mass transport from the bulk flow to the sensor surface. In this case, obtaining the inherent association and dissociation rate constants of the analyte-ligand interaction requires a model that accounts for mass transport. Therefore, we first examined the contribu-

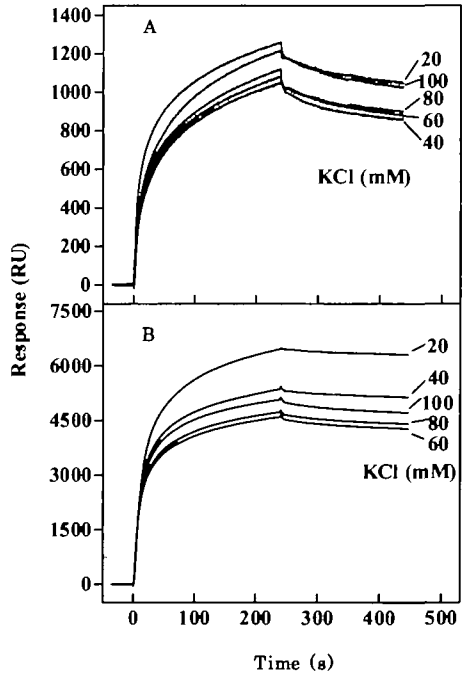

Fig. 3. **Effect of the KCl concentration on the binding of rat liver 80S ribosomes to immobilized RTA in the presence of 5 mM (A) or 15 mM (B) Mg^{2+}.** The KCl concentration in the running buffer was varied from 20 to 100 mM, as indicated in the figure. The ribosomes (100 nM) in each running buffer were injected over the RTA surface (5,450 RU immobilized) for 4 min at 5 μl/min. The dissociation of bound ribosomes was performed for 220 s with a 5 μl/min flow of the same running buffer containing no ribosomes. The responses obtained on the control surface were subtracted from those on the RTA-immobilized surfaces.

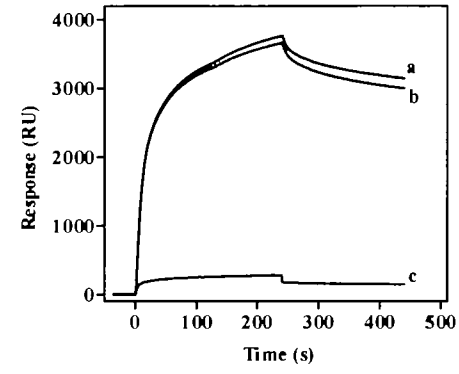

Fig. 4. **Sensorgrams obtained by injection of intact and depurinated rat liver 80S ribosomes and *E. coli* 70S ribosomes.** Ribosomes (100 nM) in the standard running buffer were injected over the surface with 4,460 RU of immobilized RTA for 4 min at the flow rate of 5 μl/min. The dissociation was performed as in Fig. 1. The responses obtained on the control surface were subtracted from those on the RTA-immobilized surfaces. a, intact rat liver 80S ribosomes; b, depurinated rat liver 80S ribosomes; c, *E. coli* 70S ribosomes.

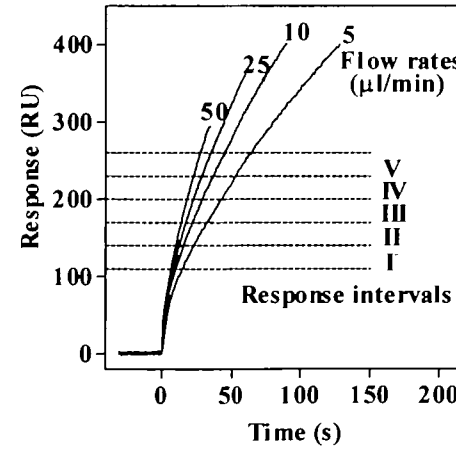

Fig. 5. **Association phases of sensorgrams obtained by injection of rat liver 80S ribosomes at four different flow rates.** Rat liver 80S ribosomes (4 nM in 40 μl of the standard running buffer) were injected over the RTA surface (4,780 RU immobilized) at flow rates of 5–50 μl/min. Five response intervals were selected, as indicated in the figure, to measure slopes (dR/dt) by linear regression.

tion of ribosomal mass transport to the observed binding rate by analyzing the effect of the flow rate on the apparent initial binding rate (dR/dt) using the BIA-CONC program based on Eq. 1 (*21*). Figure 5 shows the initial association phases of the sensorgrams obtained by injecting rat liver 80S ribosomes (4.0 nM) over the RTA surface (4,780 RU immobilized) at four different flow rates, from 5 to 50 μl/min. The slopes (dR/dt) were measured by linear regression at each response interval of 30 RU (I to V) in the range from 110 to 260 RU. The results of data analysis with a response interval of III are shown, as an example, in Table I. The response per mass per area for ribosomes (G) and the reaction flux coefficient (L_r) were calculated to be 89 RU·mm²/ng and 6.99×10^{-4} m/s, respectively, with a χ^2 value of 0.0107 according to Eq. 1 using the dR/dt_{reg}, L_m, MW, and ribosome concentration ($[A_{bulk}]$) values. The slopes (dR/dt) at each response interval were found to be approximately proportional to the cubic root of the flow rates, that is, to the mass transport coefficient L_m value, indicating that the mass transport was totally rate limiting for the observed initial binding. The total mass transport limitation was also revealed by that the reaction flux coefficient L_r values were much larger than the L_m ones, namely by the MTL values of 1.0. These results demonstrate a very high association rate for the interaction of rat liver 80S ribosomes with the immobilized RTA.

Although the initial parts of the association phases were totally mass transport-limited, the curvature of the overall association phase (Fig. 5) indicated some contribution of the intrinsic association and dissociation processes to the SPR signals. These overall data were thus analyzed with a binding model taking account of mass transport using BIAevaluation 3.0, in which the predefined model for mass transport is based on a simple two-compartment model (*26*). The mass transport rate constant k_t for rat liver 80S ribosomes was calculated to be 8.5×10^8 s^{-1} with the flow rate of 5 μl/min from the values of L_m, MW, and G for ribosomes, using Eq. 4. This predicted value of k_t, as well as other established indications, was used to assess the goodness of model-fitting to the response data. The simple 1:1 binding model was found to be unable to fit the association and dissociation data in Fig. 5, and the returned value for k_t (order of 10^{18} s^{-1}) was far from reality.

There have been a number of reports dealing with the mass transport limitation to extend the range of rate constants that can be accurately extracted from the SPR data (*23, 26, 28, 29*). Based on computer simulation data, Myszka *et al.* (*26*) have recently shown that even an association rate constant of 1×10^8 $M^{-1}s^{-1}$ can be accurately extracted with the two-compartment model. It has also been pointed out that in some cases of a high analyte molecular mass and a high receptor concentration, not only the transport of the analyte from the bulk to the gel surface but also the diffusion within the gel matrix can be a limiting factor for the binding rate (*30*). In the present system, however, the ribosomes appeared to be unable to diffuse within the gel matrix due to its too large size, as mentioned above. Thus the two-compartment model is likely to be good enough to account for mass transport. Therefore, the unsuccessful data-fitting to the simple 1:1 binding model in-

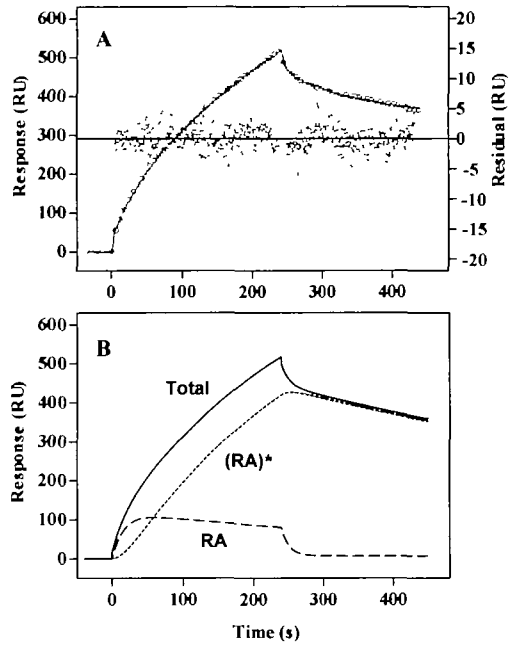

Fig. 6. **Global fitting analysis of the sensorgram obtained by injection of rat liver 80S ribosomes over the RTA surface.** (A) A solution of 4 nM ribosomes in the standard running buffer was injected over the RTA surface (5,860 RU immobilized) for 4 min at 5 μl/min, and then the dissociation was performed as in Fig. 1. The response on the control surface was subtracted from that on the RTA-immobilized surface. A global fitting curve (open circles) and residual plots (dots) for the experimental data (solid line) were calculated with the BIAevaluation 3.0 program using a two state reaction (conformational change) model taking account of mass transport. The values of the best fitted rate constants were: association (k_{a1}), (1.0 ± 0.1) × 10^8 $M^{-1}s^{-1}$; dissociation (k_{d1}), 1.9 ± 0.2 s^{-1}; forward conformational change in the complex RA (k_{a2}), (2.1 ± 0.2) × 10^{-2} s^{-1}; backward conformational change in the complex (RA)* (k_{d2}), (1.4 ± 0.1) × 10^{-3} s^{-1}; mass transport rate constant (k_t), (1.6 ± 1.3) × 10^9 s^{-1}. (B) Simulated time courses of the formation and dissociation of the initial complex RA (——), the complex (RA)* resulting from a forward conformational change in RA (····), and the total complexes (—). The parameters used for calculation of time courses were as in A.

TABLE I. **Effect of the flow rate on the slope (dR/dt) of association phases of sensorgrams with rat liver 80S ribosomes.** The association phases of sensorgrams with 4.0 nM rat liver ribosomes at different flow rates (shown in Fig. 5) were analyzed using the BIA-CONC program (*21*), and the results obtained at response interval III (170–200 RU) are shown. Slopes, dR/dt_{reg}, obtained by linear regression, are listed with χ^2 values. G and L_r values were calculated according to Eq. 1 using the dR/dt_{reg}, L_m, MW, and ribosome concentration ($[A_{bulk}]$) values as described in the text. Ideal slopes, dR/dt_{fit}, were obtained from Eq. 1 with the calculated G and L_r values. MTL is the mass transport limitation, $L_r/(L_r + L_m)$.

Response interval III (170–200 RU)	Flow rate (μl/min)	L_m (m/s)	dR/dt_{reg} (RU/s)	χ^2	dR/dt_{fit} (RU/s)	MTL
$[A_{bulk}]$ = 4.0 nM	5	2.27×10^{-6}	3.15	0.285	3.28	1.00
G = 89 RU·mm²/ng	10	2.86×10^{-6}	4.20	0.692	4.15	1.00
L_r =6.99 × 10^{-4} m/s	25	3.88×10^{-6}	5.69	0.423	5.65	0.99
χ^2 =0.0107	50	4.89×10^{-6}	7.12	0.578	7.13	0.99

cluding the two-compartment model for mass transport allowed us to conclude that the binding of ribosomes to RTA is not simple 1:1 binding. We therefore, tested more complex models as to fitting to the data.

Among the four complex models tested (see "MATERIALS AND METHODS"), a two-state reaction (conformational change) model resulted in the best fit to the experimental data with a χ^2 value of the same order of magnitude as the noise level (± 3 RU) and with a reasonable k_t (Fig. 6A). A good quality of the fit was also indicated by that the residual plots were distributed randomly. Other tested kinetic models, which may cover all possible ways of interaction between ribosomes and the immobilized RTA, resulted in obviously worse fitting to the data than the conformational change model, as judged from the χ^2 and returned k_t values as well as the residual plots. The two-state reaction model, which describes 1:1 binding of ribosomes to immobilized RTA, followed by a reversible conformational change in the complex, is expressed as:

$$R + A \underset{k_{d1}}{\overset{k_{a1}}{\rightleftharpoons}} RA \underset{k_{d2}}{\overset{k_{a2}}{\rightleftharpoons}} (RA)^* \quad (5)$$

Where R is the analyte ribosome, A is the immobilized ligand RTA, and (RA)* is the complex form after the forward conformational change in the initial complex RA. The returned values of the rate constants for association (k_{a1}), dissociation (k_{d1}), forward conformational change in the complex (k_{a2}), and backward conformational change (k_{d2}) were $(1.0 \pm 0.2) \times 10^8$ $M^{-1}s^{-1}$, 1.9 ± 0.2 s^{-1}, $(2.1 \pm 0.2) \times 10^{-2}$ s^{-1}, and $(1.4 \pm 0.1) \times 10^{-3}$ s^{-1}, respectively. If the obtained rate constant values are accurate, the data that are being fit should be sensitive to these parameters. However, changing the fixed k_{a1} value from 1.0×10^7 to 2.0×10^8 M^{-1} s^{-1} did not affect the quality of the resulting fit much, suggesting the possibility of this range of association rates. This difficulty in estimating accurate rate constants can be attributed to the fact that mass transport highly dominates the initial binding. Nevertheless, all sets of returned rate constants revealed that the ribosome first combines with RTA, an equilibrium of formation and dissociation of the initial complex RA rapidly being reached, and then a slower forward conformational change in the complex RA takes place to yield a higher-affinity complex (RA)*, thereby increasing the ribosomes bound to the RTA. This binding pathway is illustrated by the simulated time-dependent variation of the bound ribosomes in each complex form that is expressed in resonance units (RU) proportional to the mass bound to the sensor surface (Fig. 6B). In the dissociation phase, fast dissociation of RA occurs in an initial stage, followed by slower dissociation of (RA)* through a slow backward conformational change (Fig. 6B). This model (Eq. 5) is the simplest conformational change model. We also tested a more complex model that includes the additional step of direct and reversible dissociation of (RA)* to R and A. The resulting quality of the fit was not improved compared with that with the simpler original model. Thus, the additional step is not required to describe the present RTA-ribosome interaction data.

DISCUSSION

The present real-time kinetic studies on the RTA-ribosome interaction provided evidence that the higher-affinity complex of RTA and rat liver 80S ribosomes is formed through a conformational change of the initial complex. An important question regarding the mechanism of the action of RTA on ribosomes is what kind of structural rearrangement occurs in RTA and/or ribosomes that yields the higher-affinity complex after the initial binding. There have so far been a few reports that suggest a conformational change accompanying the RTA-ribosome binding. The X-ray crystallographic structures of the complexes of RTA with small substrate analogs and nucleotide ligands (*9, 31*) have revealed rotation of the side chain of Tyr80 about the Cα–Cβ bond when adenine is bound between the side chains of Tyr80 and Tyr123 at the active site cleft. This conformational shift of the Tyr80 side chain, however, may not contribute much to the complex formation observed in this study, because the mode of interaction of depurinated ribosomes (product ribosomes) was essentially the same as that of intact ribosomes (Fig. 4) and because the interaction was not influenced by the presence of 5 mM adenine, which is higher than the dissociation constant (1 mM) for the adenine-RTA complex (*27*). Thus, other parts of rRNA rather than the target adenine as well as ribosomal protein may contribute to the observed complex formation. Moreover, the interaction of RTA with rat liver 80S ribosomes may be very sensitive to the ribosomal conformation, since it was greatly affected by the Mg^{2+} concentration and ionic strength (Figs. 2 and 3).

The hairpin structure of the 29-mer S/R domain has been solved by NMR (*3, 4*) and X-ray crystallography (*5*). The conserved purine-rich sequence of 12 nucleotides in the S/R domain, which is essential for binding elongation factors (*6*), forms a GAGA tetraloop containing the target adenine (the second A) and a G-bulged cross-strand A stack. The flexible region lies between the cross-strand stack and the Watson-Crick paired stem, and has been hypothesized to participate in the ribosomal conformational change that is associated with the switch between pre- and post-translocational states (*5*). Interestingly, an induced fit mechanism has been suggested for RTA's recognizing and binding to the S/R domain by molecular dynamic simulation analysis (*32*). The induced conformational change yielding a high affinity complex has been proposed to occur in both RTA and the S/R domain as many concerted structural rearrangements that include significant positional movement of several nucleotide residues flanking the target adenine and several charged or polar amino acid residues in the RTA active site cleft. This kind of induced conformational change seems most likely to be the case in the present binding of rat liver 80S ribosomes to RTA. It was recently reported that partially unfolded inactive RTA formed on transient heating at 45°C regains full catalytic activity in the presence of salt-washed ribosomes, suggesting the ribosome-mediated refolding of RTA (*33*). Although the direct relation of this refolding phenomenon to our binding data seems not to be obvious because we used native RTA at 25°C, such a flexible conformation of RTA might facilitate the induced fit of the RTA-ribosome complex. It seems to be important for future study on the RTA-ribosome interaction that the induced conformational change of the complex will be further clarified by a combination of different analyses such as crystallography, NMR and other spectroscopies, measurement of thermodynamics, and chemical or enzymatic modification using the complex of RTA and the S/R domain nucleotides or whole ribosomes.

Concerning the pathway of the enzymatic action of RTA, it is interesting to hypothesize that a conformational change of the RTA-ribosome complex would play an activation role. If thit is true, then a slow forward conformational change has a possibility of becoming a rate-limiting step of depurination. RTA exhibits very high depurinating activity on rat liver ribosomes, but is unable to act on *E. coli* ribosomes despite the existence of the S/R domain that undergoes depurination by other RIPs such as PAP (*7, 8*). The reason for this inability of RTA to act on *E. coli* ribosomes is unknown: it may not be due to steric hindrance specific to RTA because the major structural differences between RTA and PAP do not account for their differing ribosome specificities, as concluded on peptide-swapping mutational analysis (*34*). One of the possible explanations is that the induced fit necessary for activation would not take place in the interaction of RTA with *E. coli* ribosomes. This might be due to the structure of the *E. coli* S/R domain (*35*) since it is obviously different from the rat domain in the flexible region, and may be partly due to the regions flanking the *E. coli* S/R domain including ribosomal protein L3 that interacts with PAP (*36*). The present results seem to be consistent with this assumption because detectable accumulation of the complex of *E. coli* 70S ribosomes with RTA was not observed in contrast to in the case of rat liver 80S ribosomes. In order to further establish a relationship between the kinetic parameters obtained by SPR analysis and the enzymatic activity, we are currently analyzing the interactions of rat liver 80S ribosomes with mutant RTAs having a mutation of noncatalytic residue but differing in enzymatic efficiency.

The authors wish to thank Dr. S. Ando (Saga Medical School, Japan) for providing them with the opportunity to use BIAevaluation 3.0, and Professor J.D. Robertus, Dr. A.F. Monzingo (UT at Austin, USA), and Dr. I. Okazaki (BIAcore, Japan) for the helpful discussion. They are also grateful to Professor Y. Uchida (Saga University, Japan) for his continuous encouragement.

REFERENCES

1. Lord, J.M., Roberts, L.M., and Robertus, J.D. (1994) Ricin: structure, mode of action, and some current applications *FASEB J.* **8**, 201–208
2. Endo Y., and Tsurugi, K. (1987) RNA *N*-glycosidase activity of ricin A-chain. Mechanism of action of the toxin lectin ricin on eukaryotic ribosomes. *J. Biol. Chem.* **262**, 8128–8130
3. Szewczak, A.A., Moore, P.B., Chan, Y.-L., and Wool, I.G. (1993) The conformation of the sarcin/ricin loop from 28S ribosomal RNA. *Proc. Natl. Acad. Sci. USA* **90**, 9581–9585
4. Szewczak, A.A. and Moore, P.B. (1995) The sarcin/ricin loop, a modular RNA. *J. Mol. Biol.* **247**, 81–98
5. Correll, C.C., Munishkin, A., Chan, Y.-L., Ren, Z., Wool, I.G., and Steitz, T.A. (1998) Crystal structure of the ribosomal RNA domain essential for binding elongation factors. *Proc. Natl. Acad. Sci. USA* **95**, 13436–13441
6. Moazed, D., Robertson, J.M., and Noller, H.F. (1988) Interaction of elongation factors EF-G and EF-Tu with a conserved loop in 23 S RNA. *Nature* **334**, 362–364
7. Barbieri, L., Battelli, M.G., and Stirpe, F. (1993) Ribosome-inactivating proteins from plants. *Biochim. Biophys. Acta* **1154**, 237–282
8. Hartley, M.R., Chaddock, J.A., and Bonness, M.S. (1996) The structure and function of ribosome-inactivating proteins. *Trends Plant Sci.* **1**, 254–260
9. Monzingo, A.F. and Robertus, J.D. (1992) X-ray analysis of substrate analogs in the ricin A-chain active site. *J. Mol. Biol.* **227**, 1136–1145
10. Hedblom, M.L., Cawley, D.B., Boguslawski, S., and Houston, L.L. (1978) Binding of ricin A chain to rat liver ribosomes: Relationship to ribosome inactivation. *J. Supramol. Struct.* **9**, 253–268
11. Myszka, D.G. (1997) Kinetic analysis of macromolecular interactions using surface plasmon resonance biosensors. *Curr. Opin. Biotechnol.* **8**, 50–57
12. Schuck, P. (1997) Use of surface plasmon resonance to probe the equilibrium and dynamic aspects of interactions between biological macromolecules. *Annu. Rev. Biophys. Biomol. Struct.* **26**, 541–566
13. Fivash, M., Towler, E.M., and Fisher, R.J. (1998) BIAcore for macromolecular interactions. *Curr. Opin. Biotechnol.* **9**, 97–101
14. Löfås, S. and Johnsson, B. (1990) A novel hydrogel matrix on gold surfaces in surface plasmon resonance sensors for fast and efficient covalent immobilization of ligands. *J. Chem. Soc. Chem. Commun.* 1526–1528
15. Halling, K.C., Halling, A.C., Murray, E.E., Ladin, B.F., Houston, L.L., and Weaver, R.F. (1985) Genomic cloning and characterization of a ricin gene from *Ricinus communis*. *Nucleic Acids Res.* **13**, 8019–8033
16. Lowry, O.H., Rosebrough, N.J., Farr, A.L., and Randall, R.J. (1951) Protein measurement with the folin phenol reagent. *J. Biol. Chem.* **193**, 265–275
17. Blobel, G. and Sabatini, D. (1971) Dissociation of mammalian polyribosomes into subunits by puromycin. *Proc. Natl. Acad. Sci. USA* **68**, 390–394
18. Johnsson, B., Löfås, S., and Lindquist, G. (1991) Immobilization of proteins to a carboxymethyldextran-modified gold surface for biospecific interaction analysis in surface plasmon resonance sensors. *Anal. Biochem.* **198**, 268–277
19. O'Shannessy, D.J., Brigham, B.M., and Peck, K. (1992) Immobilization chemistries suitable for use in the BIAcore surface plasmon resonance detector. *Anal. Biochem.* **205**, 132–136
20. Stenberg, E., Persson, B., Roos, H., and Urbaniczky, C. (1991) Quantitative determination of surface concentration of protein with surface plasmon resonance using radiolabeled proteins. *J. Colloid. Interface Sci.* **143**, 513–526
21. Richalet-Séordel, P.M., Rauffer-Bruyère, N., Christensen, L.H., Ofenloch-Haehnle, B., Seidel, C., and Van Regenmortel, M.H.V. (1997) Concentration measurement of unpurified proteins using biosensor technology under conditions of partial mass transport limitation. *Anal. Biochem.* **249**, 165–173
22. Christensen, L.H. (1997) Theoretical analysis of protein concentration determination using biosensor technology under conditions of partial mass transport limitation. *Anal. Biochem.* **249**, 153–164
23. Glaser, R.W. (1993) Antigen-antibody binding and mass transport by convection and diffusion to a surface: A two dimensional computer model of binding and dissociation kinetics. *Anal. Biochem.* **213**, 152–161
24. Wool, I.G. (1979) The structure and function of eukaryotic ribosomes. *Ann. Rev. Biochem.* **48**, 719–754
25. Nieuwenhuysen, P. and Clauwaert, J. (1981) Physicochemical characterization of ribosomal particles from the eukaryote Artemia. *J. Biol. Chem.* **256**, 9626–9632
26. Myszka, D.G., He, X., Dembo, M., Morton, T.A., and Goldstein, B. (1998) Extending the range of rate constants available from BIACORE: Interpreting mass transport-influenced binding data. *Biophys. J.* **75**, 583–594
27. Watanabe, K., Honjo, E., Tsukamoto, T., and Funatsu, G. (1992) Fluorescence studies on the interaction of adenine with ricin A-chain. *FEBS Lett.* **304**, 249–251
28. Schuck, P. and Minton, A.P. (1996) Analysis of mass transport-limited binding kinetics in evanescent wave biosensors. *Anal. Biochem.* **240**, 262–272
29. Karlsson, R., Roos, H., Fägerstam, L., and Persson, B. (1994) Kinetic and concentration analysis using BIA technology. *Companion Methods Enzymol.* **6**, 99–110
30. Schuck, P. (1996) Kinetics of ligand binding to receptor immobi-

lized in a polymer matrix, as detected with an evanescent wave biosensor. 1. A computer simulation of the influence of mass transport. *Biophys. J.* **70**, 1230–1249
31. Weston, S.A., Tucker, A.D., Thatcher, D.R., Derbyshire, D.J., and Pauptit, R.A. (1994) X-ray structure of recombinant ricin A-chain at 1.8 Å resolution. *J. Mol. Biol.* **244**, 410–422
32. Olson M.A. (1997) Ricin A-chain structural determinant for binding substrate analogues: a molecular dynamics simulation analysis. *Proteins* **27**, 80–95
33. Argent, R.H., Parrott, A.M., Day, P.J., Roberts, L.M., Stockley, P.G., Lord, J.M., and Radford, S.E. (2000) Ribosome-mediated folding of partially unfolded ricin A-chain. *J. Biol. Chem.* **275**, 9263–9269
34. Chaddock, J.A., Monzingo, A.F., Robertus, J.D., Lord, J.M., and Roberts, L.M. (1996) Major structural differences between pokeweed antiviral protein and ricin A-chain do not account for their differing ribosome specificity. *Eur. J. Biochem.* **235**, 159–166
35. Correll, C.C., Wool, I.G., and Munishkin, A. (1999) The two faces of the *Escherichia coli* 23 S rRNA sarcin/ricin domain: the structure at 1.11 Å resolution. *J. Mol. Biol.* **292**, 275-287
36. Hudak, K.A., Dinman, J.D., and Tumer, N.E. (1999) Pokeweed antiviral protein accesses ribosomes by binding to L3. *J. Biol. Chem.* **274**, 3859–3864